Determination of Precise Indentation Flow Properties of Metallic Materials Through Analyzing Contact Characteristics Beneath Indenter

Sung-Hoon Kim
Tel.: +(82)-2-880-8404, Fax: +(82)-2-886-4847
e-mail: iljiok@plaza.snu.ac.kr

Min-Kyung Baik
Tel: +(82)-2-880–8404, Fax: +(82)-2-886-4847
e-mail: mk98@snu.ac.kr

Dongil Kwon
Tel: +(82)-2-880-7104, Fax: +(82)-2-889-4380
e-mail: dongilk@snu.ac.kr

School of Materials Science and Engineering,
Seoul National University,
Seoul, 151-742, Korea

The continuous indentation technique is widely used for nondestructive evaluation of the mechanical properties of devices and materials. In particular, flow properties can be obtained by using this technique with a spherical indenter. Several formulas have been suggested to determine flow properties, and they commonly require the determination of the precise contact characteristics such as the contact area or depth between material and indenter to obtain the properties accurately. In this study, contact characteristics were determined by analysis of the contact morphology from FEA (finite element analysis) using mechanical property data for several steels. The contact characteristics obtained from FE simulation were compared to an analysis of the parameters of indentation load-depth curves for the steels. The contact characteristics were shown as functions of such parameters as work-hardening exponent and indentation depth. In addition, using indentation morphology from FE simulation, the flow properties were evaluated by analysis of indentation morphology for 18 materials on the basis of the two representative preexisting definitions of stress and strain, and the definitions were verified by comparison of the flow properties with tension testing data. [DOI: 10.1115/1.1865183]

1 Introduction

Flow properties such as yield strength, tensile strength, work-hardening exponent, etc. are widely used as basic design information on materials strength and as an acceptance test for materials specification. Tension tests, in which a standard specimen is subjected to a continually increasing uniaxial tensile force and specimen elongation is observed, are generally used to evaluate flow properties. However, tension tests cannot be used for safety inspection of structural units because the specimen must be extracted, which may cause failure or fracture.

The continuous indentation method using spherical indenter has been actively studied as a method for evaluating the flow properties of such various objects as materials, equipment, and structural units due to its fast, precise, and nondestructive merit. In continuous indentation tests, the load applied and the depth penetrated into the object by an indenter are continuously measured and represented as an indentation load-depth curve. Through analysis of this curve, the flow curve can be derived and flow properties can be determined.

There are some definitions of the stress and strain values, consisting of flow curves, but the precision of these definitions has not been compared and proved. Comparing the degree of the precision is possible from determination of an accurate contact area between the material and the indenter during indentation. In the real indentation test, elastic deflection and plastic pile-up/sink-in behaviors of the material make it difficult to determine an accurate contact area.

In this study, the contact area could be determined from indentation morphology by FE simulation based on simulation conditions that accurately reflect the conditions of actual indentation tests. The contact area results were compared with those from equations suggested by previous research. In addition, using the contact area from the FE simulation, flow curves obtained from the stress-strain definitions were compared with those from the tensile test. Through these results, the superiority between the definitions of stress-strain can be analyzed.

2 Theoretical Background

2.1 Indentation Load-Depth Curve. The indentation load-depth curve is obtained from a continuous indentation test, as shown in Fig. 1. The single indentation load-depth curve in Fig. 1(*a*) includes one loading curve and one unloading curve. The maximum depth $h_{\max}$ is the total displacement of the material and the indenter at maximum load $L_{\max}$ including elastic and plastic deformation. In unloading, the elastic deformation is fully recovered and the initial slope of the unloading curve is the indentation stiffness of the specimen and the indenter, S [9,10]. The final depth h_f is the plastic deformation of the material.

Doerner and Nix [10] showed that the elastic modulus could be evaluated by this test, and Oliver and Pharr [9] established a method to evaluate the elastic modulus and load-on hardness. However, work is ongoing to evaluate other mechanical properties such as fracture toughness, flow properties, viscoelastic properties, and residual stress. Among these properties, methods for evaluating flow properties are of interest in some industrial fields because they can be used for materials with local property gradients and for materials in service.

2.2 Evaluation of Indentation Flow Properties. Indentation flow properties are the flow properties obtained from analysis of the indentation load-depth curve. This technique starts from the premise that materials behave similarly in the tensile and compressive loading state. The flow curves of many materials undergoing uniform plastic deformation can be expressed by the following simple power-curve relation:

$$\sigma = K\varepsilon^n \tag{1}$$

Contributed by the Materials Division for publication in the JOURNAL OF ENGINEERING MATERIALS AND TECHNOLOGY. Manuscript received February 11, 2004; revision received October 23, 2004, Review conducted by: A. Pelegri.

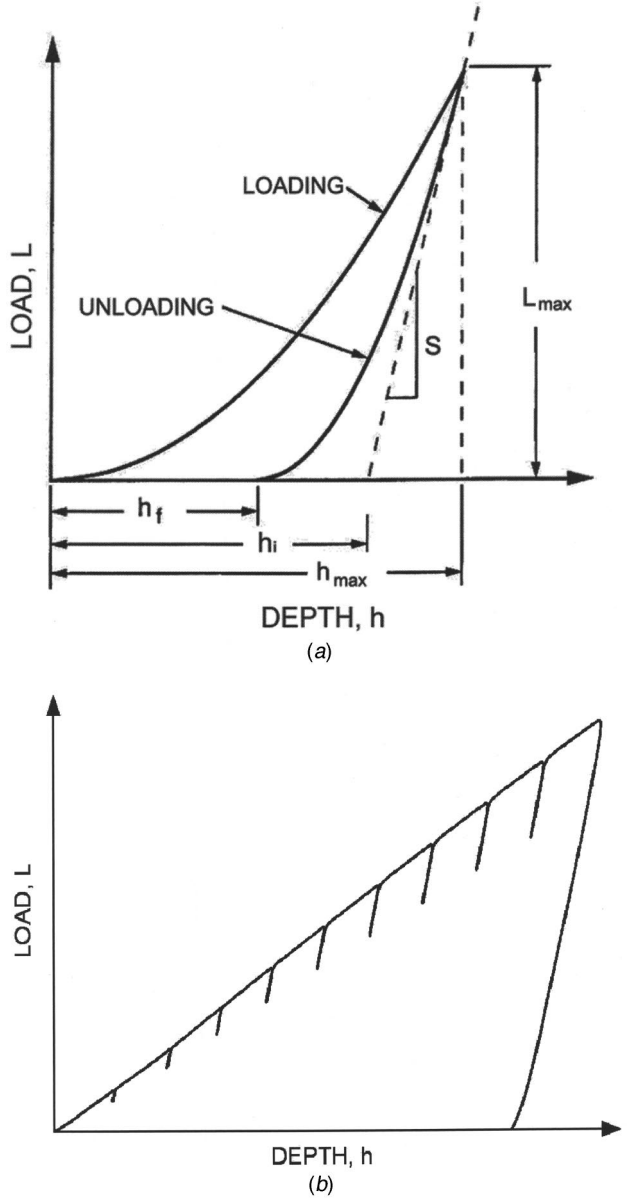

Fig. 1 Indentation load-depth curves: (*a*) single and (*b*) multiple indentation curve

where σ is the true stress, ε is the true strain, n is the work-hardening exponent, and K is the strength coefficient.

The strain produced in a material is a dimensionless parameter describing a fractional change in shape [11]. The shape is determined by the ratio d/D, where d is the residual imprint diameter and D is the indenter diameter. The flow strain ε has been expressed by Tabor [11] as

$$\varepsilon = 0.2\frac{d}{D} = 0.2\sin\gamma \tag{2}$$

Since the maximum strain that can be obtained from Eq. (2) is 0.2, this equation has the limitation that it cannot be used to describe the flow strain for materials with very large strain or elongation. Ahn et al. [1] suggested a new equation based on the idea that the displacement of the indenter-penetration direction (z-direction) can be obtained from the geometrical shape of the indenter and the strain can be obtained by differentiation of the displacement relation:

$$\varepsilon = \frac{\alpha}{\sqrt{1-(d/D)^2}}\frac{d}{D} = \alpha\tan\gamma, \tag{3}$$

where α is a constant, generally 0.12 [12].

The flow stress can be obtained from the relation with the mean contact pressure P_m defined as

$$P_m = \frac{L}{A_c} \tag{4}$$

where L is the applied load and A_c, the projected contact area between indenter and material, is a function of d. The relation can be expressed, with the introduction of the plastic constraint factor ψ, as [1,6,11,13]

$$\sigma = \frac{P_m}{\psi} \tag{5}$$

where ψ is a value changing with deformation characteristics, such as elastic, elastoplastic, and fully plastic.

2.3 Determination of the Contact Area (or Depth) From Indentation Load-Depth Curve. The contact area A_c is a function of d and d is a function of the contact depth h_c. The contact depth is thus the basic datum for determining such flow properties as stress and strain. The contact depth is, however, difficult to obtain due to the elastic deflection and plastic deformation of material around the indenter, as shown in Fig. 2. Plastic deformation occurs in two forms, pile-up [Fig. 2(*a*)] and sink-in [Fig. 2(*b*)]; the contact area between the material and the indenter is increased by pile-up but decreased by sink-in.

The elastic deflection decreases the contact area and the amount of the deflection. The following equation has been suggested for the deflection depth h_d [9]:

$$h_d = \omega\frac{L_{\max}}{S} \tag{6}$$

where S is stiffness, the initial slope of the unloading curves, and ω is a constant related to the shape of the indenter. Using the depth relation, Oliver and Pharr [9] suggested that

$$h_c^* = h_{\max} - h_d \tag{7}$$

where h_c^* is the contact depth ignoring the pile-up/sink-in phenomena.

The increase or decrease in the contact area by plastic deformation is known to be a function of the work-hardening exponent, the ratio of yield strength to elastic modulus and the ratio of the penetration depth to the indenter radius [14–18]. Early research on the phenomena studied primarily the effect of the work-hardening exponent. Norbury and Samuel [16] suggested that the amount of pile-up or sink-in could be expressed as a percentage of the depth and the percentage pile-up or sink-in constants were related to the work-hardening exponent n. Subsequent research led to the following relationship between the amount of pile-up/sink-in and the work-hardening exponent [17,18]

$$\frac{s}{h_{\max}} = \frac{1}{2}\left(\frac{2+n}{2}\right)^{2(1/n-1)} - 1 \quad [17] \tag{8}$$

$$\frac{s}{h_{\max}} = \frac{5}{2}\left(\frac{2-n}{4+n}\right) - 1 \quad [18] \tag{9}$$

where s, the amount of pile-up/sink-in, can be expressed as $h_{pile} - h_d$, as shown in Fig. 3. On the basis of these results, the contact depth h_c for pile-up can be expressed as

$$h_c = h_{\max} - h_d + h_{pile} \tag{10}$$

where h_{pile} is the pure plastic amount of pile-up/sink-in excluding elastic deflection. Finally, the contact area is defined from the geometrical relation of the contact area and contact depth:

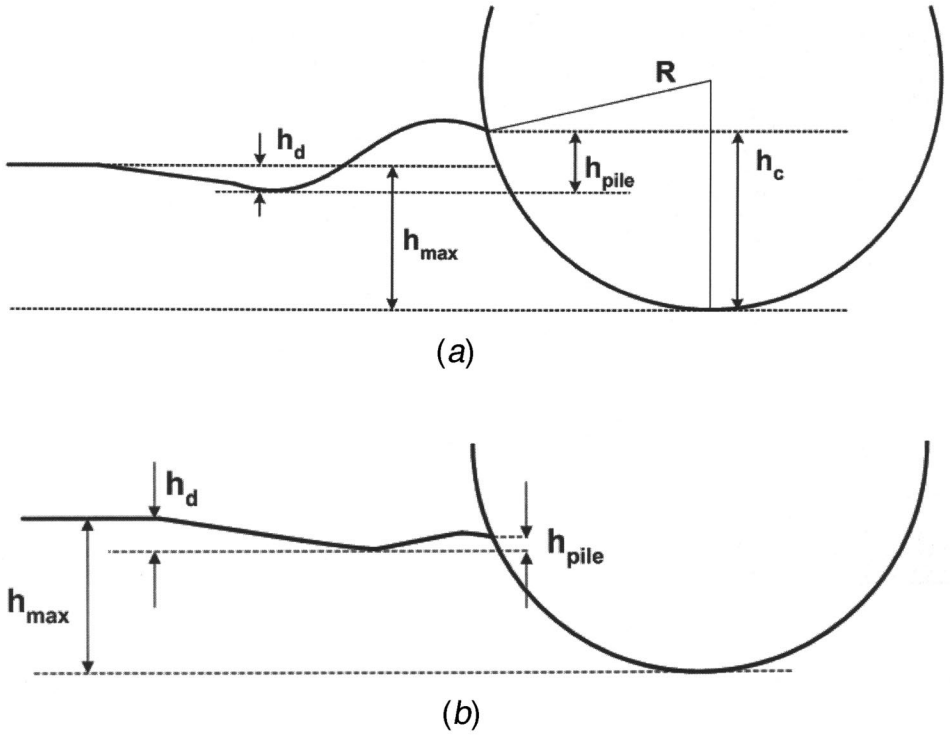

Fig. 2 Deformation phenomena around the indenter; (*a*) pile-up and (*b*) sink-in

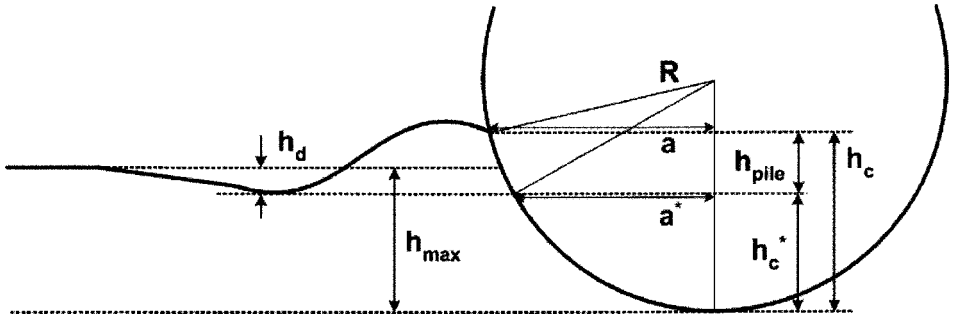

Fig. 3 Contact morphology and definitions of depth values

Table 1 Materials used in this study

Material	Al2011	API X42	API X65	KP	NAK	SA508
	Aluminum Alloy	Pipe Steel	Pipe Steel	Pipe Steel	Plastic Mold Steel	Pressure Vessel Steel
	SCM21	SCM440	S45C	SK3	SK4	SKD11
	Structural Steel	Structural Steel	Structural Steel	Tool Steel	Tool Steel	Tool Steel
	SKD61	SKH51	SS400	SUJ2	SUS304	SUS316
	Tool Steel	Tool Steel	Structural Steel	Bearing Steel	Stainless Steel	Stainless Steel

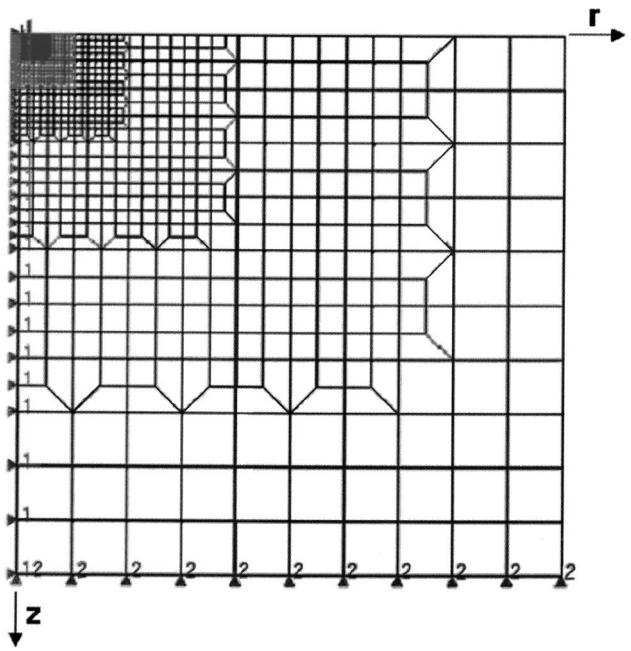

Fig. 4 The finite element mesh

$$A_c = \pi a^2 = \pi(2Rh_c - h_c^2) \tag{11}$$

where a is the contact radius and R is the radius of the spherical indenter.

3 Experimental Procedures

3.1 Continuous Indentation Test. The materials tested were the 17 industrial steels and the one aluminum alloy as listed in Table 1. The specimens were cut to $25\times25\times20$ mm, ground, and polished with 1 μm alumina. Continuous indentation tests were performed for each material using Frontics, Inc.'s AIS2000 equipment with a spherical indenter of 0.5 mm radius made of tungsten carbide (WC). Each experimental condition was selected as loading and unloading rate 0.3 mm/min, maximum indentation depth 250 μm, number of unloadings 10, and unloading rate 30%.

3.2 Finite Element Analysis. Simulation of the indentation process was carried out using ABAQUS finite element code. An axisymmetric FE analysis was employed with the indenter modeled as a rigid spherical ball. A cylindrical specimen of diameter 200 mm and height 100 mm was modeled with 3738 linear four-node elements; indenter diameter was 1 mm. The indentation depth was selected as 250 μm, as in the indentation test. A cylindrical coordinate system with radial coordinate r and axial coordinate z was used. As shown in Fig. 4, the bottom surface of the specimen has the z displacement fixed, whereas free movement is allowed in the r direction. The appropriate boundary conditions for modeling the axisymmetric behavior were applied along the centerline, and a free surface was modeled at the top and outside surface of the specimen. A friction coefficient μ of 0.2 was used in the computations to model the behavior of the indenter/specimen interface.

The basic input material properties were the true stress-true strain curves, elastic modulus, and Poisson's ratio for each material listed in Table 2. Tensile properties were measured from ten-

Table 2 Mechanical properties measured for the materials used in this study

Material	Yield Strength [MPa]	Tensile Strength [MPa]	Work-hardening Exponent	Elastic Modulus [GPa]	Poisson's Ratio
Al2011	270.00	474.00	0.1858	74.09	0.3355
API X42	436.20	619.70	0.1440	206.52	0.2969
API X65	494.72	647.39	0.1532	216.28	0.2687
KP	765.50	1003.40	0.1237	211.18	0.2861
NAK	1207.44	1358.98	0.0508	202.62	0.2868
SA508	638.42	960.39	0.1376	201.67	0.2957
SCM21	279.53	628.97	0.2057	208.83	0.2684
SCM440	654.07	1027.22	0.1598	210.64	0.2885
S45C	374.14	920.13	0.3378	209.05	0.2873
SK3	244.10	690.70	0.2640	208.74	0.2929
SK4	311.15	833.14	0.2115	209.15	0.2908
SKD11	242.90	932.10	0.2759	215.66	0.2942
SKD61	350.25	901.21	0.2910	221.48	0.2676
SKH51	263.85	920.13	0.2591	246.80	0.2411
SS400	272.70	514.36	0.2345	211.26	0.2984
SUJ2	322.80	795.30	0.2442	214.85	0.2864
SUS304	306.40	1076.71	0.3418	197.95	0.2901
SUS316	366.65	956.93	0.2806	197.16	0.2913

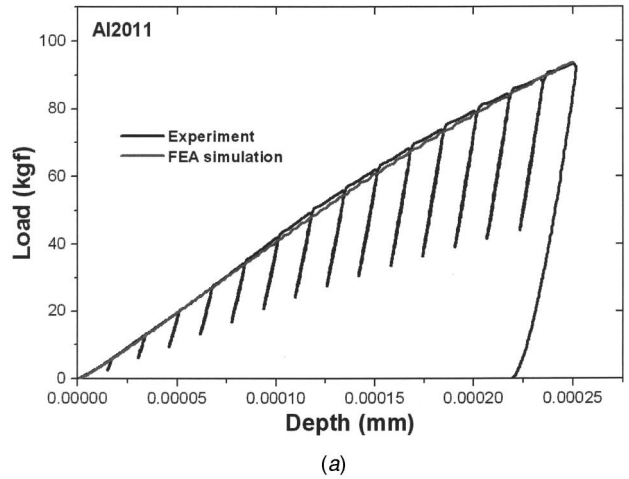

(*a*)

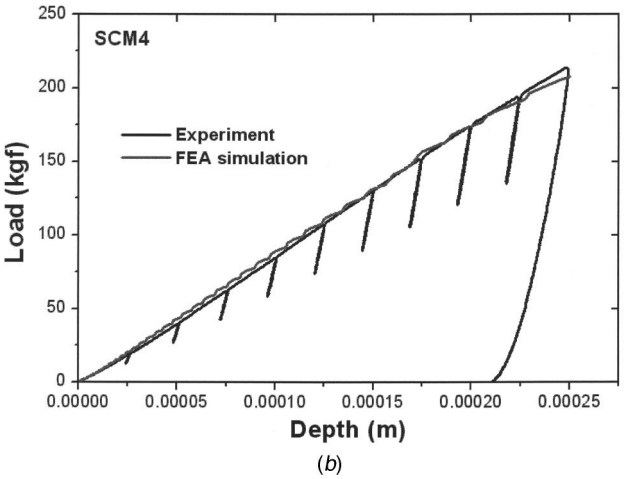

(*b*)

Fig. 5 Indentation load-depth curves from continuous indentation tests and from FE simulation: (*a*) Al2011 and (*b*) SCM4

sile tests using the Instron 5582 on the basis of ASTM E8-00. Elastic modulus and Poisson's ratio were measured by the ultrasonic method using Tektronics, Inc.'s TDS220.

4 Results and Discussion

4.1 Determination of Contact Area Considering Pile-up. To verify the reliability of the indentation load(L)-depth(h) curves and indentation morphologies obtained from FE simulation, the L-h curves were compared with those from real indentation tests (see Fig. 5). The figure shows that indentation load-depth curves from FE simulation were very similar to those from continuous indentation tests, so that the results of indentation morphology obtained from FE simulation are considered reliable.

It was observed from the simulation results for 18 materials that pile-up height was dependent on indentation depth and work-hardening exponent. This is shown in Fig. 6 for the materials used here with work-hardening exponents ranging from 0 to 0.4.

Here s/h is the pile-up parameter, where s is the pile-up height from the original plane and h is the depth of penetration into the specimen from the original plane. For small indentation depths, the relation between the pile-up parameter and the work-hardening exponent is described well by the equation (9) suggested by Hill [18]. However, the relation deviates from this equation with increasing depth and shows a linear inverse proportion: for indentation depths over 200 μm, the relationship suggested by Hill is not suited to metallic materials with a work-hardening exponent less than 0.4, but the linear relationship suggested by Rhee and McClintock [15] works well. Also, the pile-up parameter increased with increasing indentation depth, as shown in Fig. 7; this figure also shows that the pile-up parameter decreases with increase of work-hardening exponent.

In addition, the pile-up parameter either was not related to the inverse yield strain (the ratio of elastic modulus to yield strength)

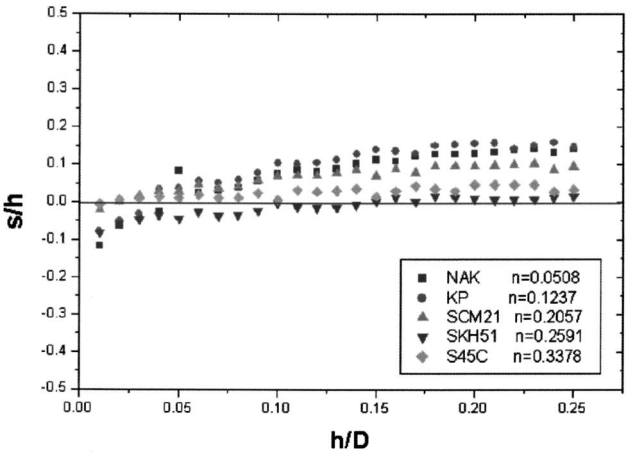

Fig. 7 Influence of penetration depth on pile-up parameter for five materials

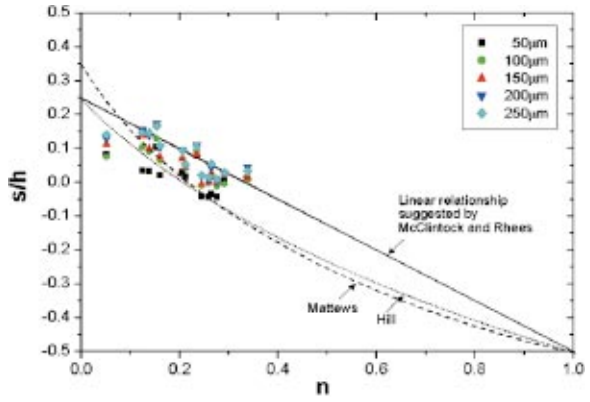

Fig. 6 Correlation between the pile-up parameter *s*/*h* and the work-hardening exponent *n*

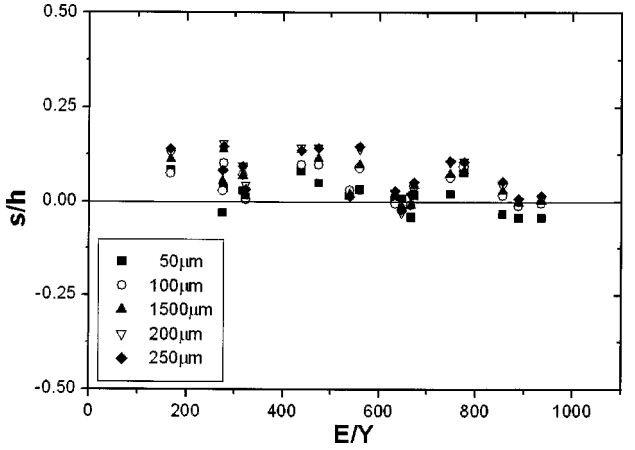

Fig. 8 Correlation between pile-up parameter *s*/*h* and yield ratio *E*/*Y*

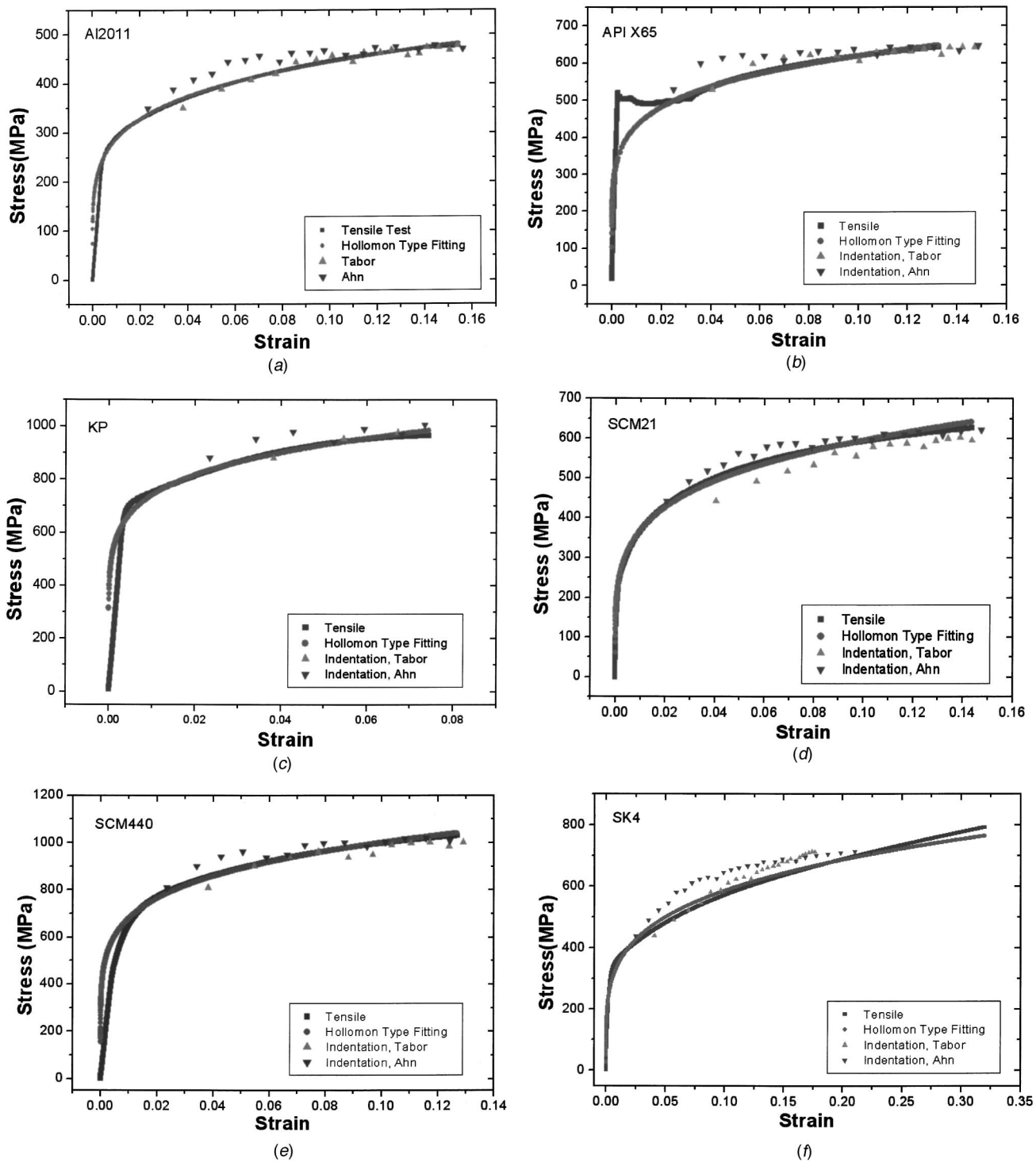

Fig. 9 Comparison of flow curves from continuous indentation tests and those from tensile tests for nine materials

E/Y or was in somewhat inverse proportion to it, as shown in Fig. 8. According to the previous FE research for E/Y effect [14,19], the pile-up parameter was increased with the increase of E/Y value if other parameters such as h/D and n are fixed. But in this study considering the effect of all parameters, the E/Y effect was different from the previous one and not clear.

It is thus confirmed that a new relationship must be introduced as a function of indentation depth, in addition to that for the work-hardening exponent suggested by Hill, Mattews, and McClintock, in order to determine the precise contact depth (or area). In addition, study about the E/Y effect should be performed for more materials having the different n and E/Y in order to clarify the effect in company with consideration of n and h/D effects.

4.2 Derivation of Flow Stress and Strain. In this study the contact area was directly obtained from the contact morphology between the indenter and the material, obtained from FE simulation. As discussed above, several equations have been suggested to express the stress and strain value. Of these, two equations suggested by Tabor [11] and Ahn [1] were verified in this study, since the definitions of stress are very similar.

For 9 of our 18 materials, the stress-strain results evaluated by

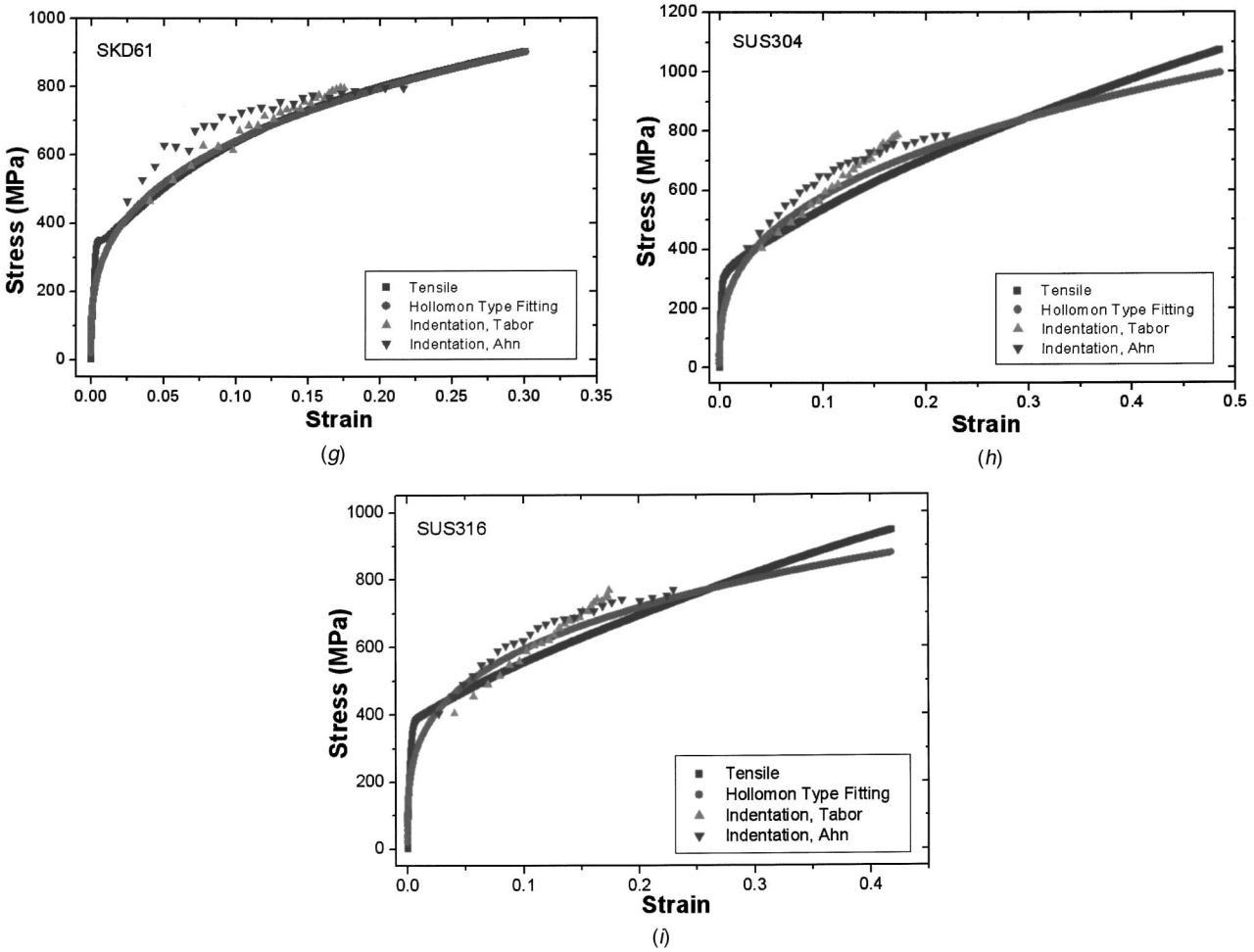

Fig. 9 (***continued***)

FE simulation morphology were compared with those evaluated by tension test. The results are superposed in Fig. 9. In these figures, generally, the results using Eq. (2) defined by Tabor agreed better with the tensile results than those using Eq. (3) by Ahn. The results using Eq. (2) described work-hardening behavior similar to that of the actual material. However, Tabor's definition of strain has the limitation that it cannot express strain values over 0.2 (when indentation is performed to the same depth as indenter radius R). Therefore, to apply Tabor's equation to materials with large strain values, the strain over 0.2 must be extrapolated.

The results obtained from the equation (3) suggested by Ahn showed less good agreement with the tensile results than those from Eq. (3). However, this definition of strain can express strain values larger than 0.2. In addition, for stainless steel, Ahn's definition reflected the flow characteristics of the materials under large strain.

The stress and strain values obtained here by the two definitions from the FE simulation results showed Hollomon-type work-hardening behavior and that stress and strain have the relation like Eq. (1), probably because the definitions were suggested on the basis of such behavior. Using these characteristics, the yield and the ultimate tensile strength (UTS) were directly determined from the indentation test. Data points of stress-strain obtained from Tabor and Ahn's definitions were fitted as the Hollomon type. The indentation strength values were determined as the stress for the same strains as yield strain and tensile strain in the tension test. Flow curves for the material having large elongation were obtained by extrapolation of the Hollomon-type fitting. The results from the indentation test were compared with that from the tension test as shown in Fig. 10.

The strength results obtained from the indentation test had good accordance with the results from the tension test. In particular, ultimate tensile strength values have the error within 5% for the results from the tension test. But, in the case of yield strength, the results presented relatively large error compared with those for UTS results. Yield strength is affected on data points of stress and strain obtained by analyzing the former unloading parts of the multiple indentation load-depth curve. The number of unloading as 15 was not enough to precisely determine the yield strength of the materials having small values because the strain value by first unloading, the nearest value from the yield strain, is even larger than the yield strain. Hence increasing the number of unloading, especially in the low load range, can be helpful to decrease the error by describing well the initial plastic deformation behavior of the material.

Meanwhile the yield strength values obtained from Tabor's definition were commonly smaller than those obtained from the tension test for the most of materials. This means the yield strength value should be determined for the larger yield strain than that from the tension test. The yield strain from the tension test cannot be used to determined the yield strength from the indentation test using Tabor's definition. Therefore, a new definition of yield strain for the indentation test should be suggested to determine yield strength from the indentation test using Tabor's definition.

5 Conclusions

Research on evaluating the flow curves of materials and structural units has used the continuous indentation technique with a spherical indenter, and contact characteristics must be analyzed to do this precisely. However, since it is difficult to measure the

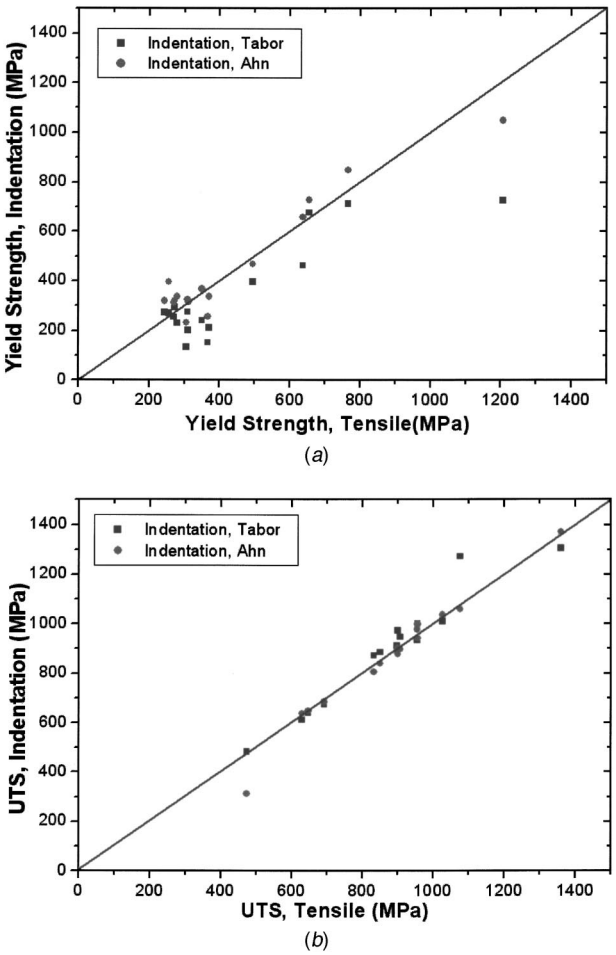

Fig. 10 Comparison of flow properties from continuous indentation tests and those from tensile tests

contact characteristics directly, in this study FE simulation was used, with tensile testing results used as the basic simulation data. Contact morphologies and load-depth curves were obtained from the simulation and previously suggested definitions of stress and strain were verified by analyzing them.

Since contact depth values affect stress and strain values, they must be determined precisely by taking into account indentation morphology. The definitions suggested by such previous researchers as Hill and Matthews are functions of the work-hardening exponent only. The results of this study show that the pile-up parameter changed with increasing indentation depth, so that new definitions including indentation depth as well as work-hardening exponent are needed.

In addition, the definition of stress and strain suggested by Tabor describes work-hardening behavior well but cannot be applied to the behavior of materials having large tensile strains due to the limitation of the maximum value. On the other hand, Ahn's definition can be applied to the work-hardening behavior of materials having large tensile strains and also can describe the work-hardening behavior of stainless steels.

Acknowledgments

This work was supported in part by the Korean Ministry of Science and Technology under the National Research Laboratory (NRL) Program.

Nomenclature

a^* = Contact radius not considering pile-up
a = Contact radius considering pile-up
D = Indenter diameter
d = Mean diameter of the imprint
d_m = Mean diameter of the imprint measured by optical microscopy or profiler
d_{m0} = Diameter of the imprint measured for original surface
d_{mp} = Diameter of the imprint measured for the top point of pile-up
E = Elastic modulus
h_d = Deflection depth
h_f = Final depth
$h_{\max}$ = Maximum depth
h_{pile} = Pile-up height
L = Indentation load
$L_{\max}$ = Maximum indentation load
n = Work-hardening exponent
R = Radius of curvature of residual imprint
Y = Yield strength

References

[1] Ahn, J.-H., and Kwon, D., 2001, "Derivation of plastic stress-strain relationship from ball indentation: Examination of strain definition and pileup effect," J. Mater. Res., **16**, pp. 3170–3178.
[2] Haggag, F. M., 1993, "In-situ measurements of mechanical properties using novel automated ball indentation system," ASTM STP 1204, Philadelphia, pp. 27–44.
[3] Suresh, S., and Giannakopoulos, A. E., 1998, "A new method for estimating residual stresses by instrumented sharp indentation," Acta Mater., **46**(16), pp. 5755–5767.
[4] Lee, Y.-H., and Kwon, D., 2002, "Residual stresses in DLC/Si and Au/Si systems: application of a stress-relaxation model to the nanoindentation technique," J. Mater. Res., **17**(4), pp. 901–906.
[5] Malzbender, J., and de With, G., 2000, "Energy dissipation, fracture toughness and the indentation load-displacement curve of coated materials," Surf. Technol., **135**, pp. 60–68.
[6] Murty, K. L., Mathew, M. D., Wang, Y., Shah, V. N., and Haggag, F. M., 1998, "Nondestructive determination of tensile properties and fracture toughness of cold worked A36 steel," Int. J. Pressure Vessels Piping, **75**(11), pp. 831–840.
[7] Asif, S. A. S., Wahl, K. J., and Colton, R. J., 1999, "Nanoindentation and contact stiffness measurement using force modulation with a capacitive load-displacement transducer," Rev. Sci. Instrum., **70**(3), pp. 2408–2413.
[8] Lucas, B. N., Oliver, W. C., and Swindeman, J. E., 1998, "The dynamics of frequency-specific, depth-sensing indentation testing," in *Fundamentals of Nanoindentation and Nanotribology*, N. R. Moody et al., eds., MRS, Warrendale, PA, Vol. 522, pp. 3–14.
[9] Oliver, W. C., and Pharr, G. M., 1992, "An improved technique for determining hardness and elastic modulus using load and displacement sensing indentation experiments," J. Mater. Res., **7**(6), pp. 1564–1583.
[10] Doerner, M. F., and Nix, W. D., 1986, "A method for interpreting the data from depth-sensing indentation instruments," J. Mater. Res., **1**(4), pp. 601–616.
[11] Tabor, D., 1951, *Hardness of Metals*, Clarendon Press, Oxford, p. 2.
[12] Jeon, E.-c., Park, J.-S., and Kwon, D., 2003, "Statistical Analysis of Experimental Parameters in Continuous Indentation Tests Using Taguchi Method," ASME J. Eng. Mater. Technol., **125**, pp. 406–411.
[13] Francis, H. A., 1976, "Phenomenological Analysis of Plastic Spherical Indentations," Trans. ASME, July, pp. 272–281.
[14] Taljat, B., and Pharr, G. M., 1998, "Pile-up behavior of spherical indentations in engineering materials," Mater. Res. Soc. Symp. Proc., **522**, pp. 33–38.
[15] Rhee, S. S., and McClintock, F. A., 1962, "On the effect of strain hardening on strain concentrations," *Proc. 4th US Nat. Conf. Applied Mechanics*, ASME, Berkeley, CA.
[16] Norbury, A. L., and Samuel, T., 1928, "The recovery and sinking-in or piling-up of material in the brinell test, and the effects of these factors on the correlation of the brinell with certain other hardness tests," J. Iron Steel Inst., London, **117**, pp. 673–687.
[17] Matthews, J. R., 1980, "Indentation hardness and hot pressing," Acta Metall., **28**, pp. 311–318.
[18] Hill, R., Storkers, B., and Zdunek, A. B., 1989, "A theoretical study of the Brinell hardness test," Proc. R. Soc. London, Ser. A, **23**, pp. 301–330.
[19] Cheng, Y. T., and Cheng, C. M., 1998, "Effect of sinking in and piling up on estimating the contact area under load in indentation," Philos. Mag. Lett., **78**, pp. 115–120.